ACS APPLIED MATERIALS & INTERFACES

Research Article

www.acsami.org

Strategies for Stabilization of Electrodeposited Metal Particles in Electropolymerized Films for H_2O Oxidation and H^+ Reduction

Daniel A. Torelli,[‡] Daniel P. Harrison,[†] Alexander M. Lapides,[‡] and Thomas J. Meyer*[,‡]

[‡]Department of Chemistry, University of North Carolina at Chapel Hill, CB 3290, Chapel Hill, North Carolina 27599-3290, United States

[†]Department of Chemistry, Virginia Military Institute, Lexington, Virginia 24450, United States

Supporting Information

ABSTRACT: Metal particles were electrodeposited on a variety of conducting substrates, and their electrocatalytic activity toward H_2O oxidation to O_2 and H^+ reduction to H_2 was evaluated. Co, Ni, Cu, Pd, Ag, and Pt were all electrodeposited on fluorine-doped tin oxide (FTO) electrodes. Particularly active were Pd and Pt for H^+ reduction and Co and Ag for H_2O oxidation. When cycled reductively in 0.1 M $HClO_4$, FTO electrodes derivatized with Pt and Pd reached current densities for hydrogen evolution of 18.3 and 13.2 mA/cm^2, respectively, at −0.6 V vs normal hydrogen electrode (NHE). FTO electrodes with electrodeposited Co or Ag were cycled oxidatively in H_2O buffered to pH 7 with phosphate buffer. Current densities of 10.5 and 8.70 mA/cm^2, respectively, were reached at +1.8 V vs NHE with H_2O oxidation onsets at +1.3 and +1.4 V, respectively. The impacts on catalytic stability and performance of electrodeposited metals in/on an electrically conductive polymer support were also investigated. Films of poly-[Fe(vbpy)$_3$](PF$_6$)$_2$ (vbpy is 4-methyl-4′-vinyl-2,2′-bipyridine) were generated on FTO by reductive electropolymerization. Significant improvements to the long-term stability of electrodeposited Ag and Pt particles were observed in the poly-[Fe(vbpy)$_3$](PF$_6$)$_2$ support. Films of poly-[M(vbpy)$_3$](PF$_6$)$_2$ with M = Co(II) or Cu(II) were also prepared and evaluated as electrocatalysts for H_2O oxidation. Films containing Co(II) reached current densities of 6.0 mA/cm^2 at +1.8 V vs NHE in H_2O.

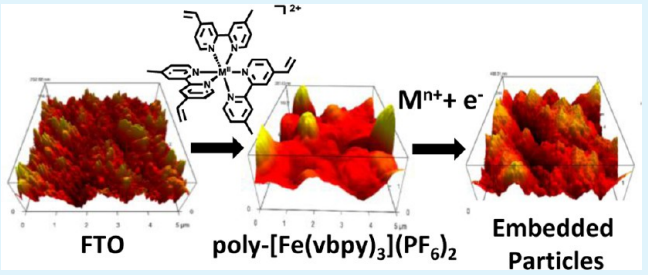

KEYWORDS: *water oxidation, proton reduction, electrocatalysis, heterogeneous catalysis, electrodeposition, electropolymerization*

INTRODUCTION

There is a well-documented need for electrocatalysts for energy applications in energy storage and solar fuels.[1−5] We report here a general method for forming interfacial structures for possible applications in electrocatalytic and photoelectrocatalytic water oxidation to oxygen and proton reduction to hydrogen. Our approach utilizes electrodeposition of dispersed nanoparticles on a variety of electrode surfaces and at modified interfaces. Of particular interest are the first and second row transition metals such as Co, Cu, and Ag as possible alternatives to more expensive precious metals such as Ir, Pt, and Pd.

In addition to direct electrodeposition, we have explored the impact on reactivity and catalytic stability of incorporating catalytically active metal particles in/on preformed metal complex-containing polymeric films. The films are prepared by reductive electropolymerization of vinyl-derivatized metal complexes, Scheme 1, followed by electrodeposition of the particles.[6−8] Three film-based incorporation strategies have been explored: (1) electrodeposition of metals on/into films of poly-[Fe(vbpy)$_3$](PF$_6$)$_2$ (vbpy is 4-methyl-4′-vinyl-2,2′-bipyridine), (2) prior coordination of metal ions or complexes to CN^- and free bpy ligands in poly-Fe(vbpy)$_2$(CN)$_2$,poly-vbpy,[6,7] and (3) replacement of Zn^{2+} ion in preformed films of poly-[Zn(vbpy)$_3$](PF$_6$)$_2$ by external cations to give films of poly-[M(vbpy)$_3$](PF$_6$)$_2$.[8] Polymeric film structures are illustrated in Figure 1.

Scheme 1. Electropolymerization

$$Fe^{II}(vbpy)_3^{2+} + e^- \rightarrow Fe^{II}(vbpy)_2(vbpy^{\cdot-})^+$$

$$Fe^{II}(vbpy)_2(vbpy^{\cdot-})^+ + Fe(vbpy)_3^{2+} \rightarrow Fe(vbpy)_2bpy\text{-}CRH\text{-}CH_2\text{-}CRH\text{-}bpyFe(vbpy)_2$$

$$\rightarrow\rightarrow \xrightarrow{-e^-} poly\text{-}[Fe(vbpy)_3]^{2+}$$

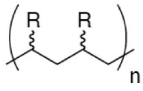

R = Fe(vbpy)$_2$(bpy)$^{2+}$

The metal complex-based films are electrically conductive but at potentials dictated by the redox potentials of the $Fe^{III/II}$ couple ($E_{1/2}$ = 0.70 V vs Ag/AgNO$_3$ in CH_3CN) and ligand-based (bpy$^{-/o}$) couple at $E_{1/2}$ = −1.8 V. Films of the vinyl-containing complexes are formed on any conducting substrate by well-established reductive electropolymerization proce-

Received: April 11, 2013
Accepted: June 27, 2013
Published: June 27, 2013

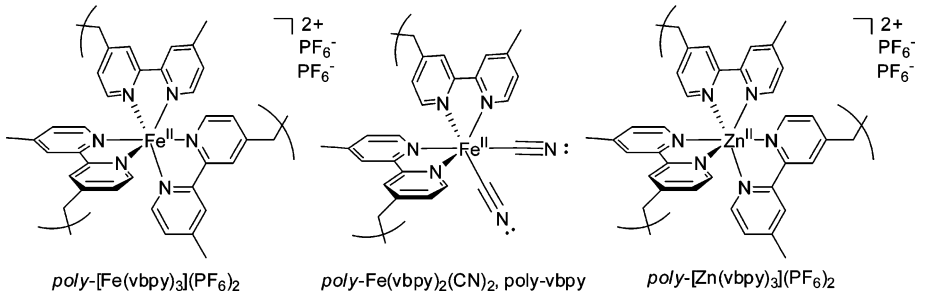

Figure 1. Structures of the monomer units in films derived from poly-$[M(vbpy)_3](PF_6)_2$ (M = Fe(II), Zn(II)).

dures.[6−19] In this process, the potential of the underlying electrode is scanned to sufficiently negative potentials to reduce the complexes at π^* levels on the vbpy ligands which induces vinyl polymerization, Scheme 1. The mechanism involves reduction and vinyl radical polymerization in the double layer near the electrode.[6] With multiple polymerizable vinyl substituents, polymerization is accompanied by extensive cross-linking and insoluble polymer films that are deposited on the electrode surface. The rate of film growth and film thickness can be controlled by varying the concentration of complex in the solution, the scan rate in voltammetric scans, the number of scan cycles, and the potential range used in reductive scans.

This study focused on utilizing the resulting polymer films as semiporous supports for small metallic particles formed by electrochemical reduction at the electrode−film interface. Metal particles were deposited by diffusion of external metal ions into and through the films to the electrode interface where they undergo reduction. In the resulting modified films, small metal particles form both on the surface and inside the films, effectively increasing the catalytically active surface area compared to electrodeposition on a bare electrode.

In a second approach, an element of coordination control was introduced by converting poly-$[Fe(vbpy)_3](PF_6)_2$ into poly-$Fe(vbpy)_2(CN)_2$,poly-vbpy, with the −CN ligands and uncoordinated vbpy groups available for concentrating and coordinating metal ions prior to reduction.[6,7] In a third approach, labile Zn(II) ions in films formed by reductive electropolymerization of $[Zn(vbpy)_3](PF_6)_2$ to give poly-$[Zn(vbpy)_3](PF_6)_2$ are substitutionally labile and undergo exchange with divalent cations added to the external solution. This provides an additional strategy for metal ion concentration and coordination within the film structure prior to reduction. In this study, this approach was used to exchange Zn(II) in preformed films with Co^{2+}, Fe^{2+}, and Cu^{2+} ions in the external solution which are redox active at accessible potentials and participate in electrocatalysis.[8]

There is an extensive literature on electrodeposition and catalysis by electrodeposited metals.[20] The strategy introduced here is distinct in that most previous work has focused on oxidative electrodeposition of metal oxides, reductive electrodeposition on bare electrodes, or electrodeposition in conducting polymers such as polypyrrole.[20−26] There is precedence for the incorporation of metal ions[6−8] and/or metal complexes[27] into metal complex-based electropolymerized polymer films for applications in electrocatalysis. The focus of these studies was on incorporation strategies rather than electrocatalytic reactivity and stability. In the strategy adopted here, a redox active metal is incorporated in the initially formed polymer film allowing for characterization of the film by electrochemical and spectroscopic methods while providing a semiporous network to support metal particle deposition to improve long-term stability.

EXPERIMENTAL SECTION

Electrochemistry. Electrochemical experiments were performed in a 3-compartment glass cell separated by medium or fine porosity frits. A fluorine-doped tin oxide (FTO) electrode was suspended in the center compartment with the middle of the electrode wrapped in Kapton tape to create a well-defined surface area of 1.0 cm^2. FTO was cleaned by two sonication cycles in isopropanol for 20 min followed by 2 × 20 min sonication sequences in Milli-Q H_2O and air-dried. In the electropolymerization experiments, the electrodes were sonicated in CH_3CN for 15 min and rinsed with CH_3CN. Electropolymerizations and electrodepositions were conducted in Optima CH_3CN 0.1 M in $TBAPF_6$ (tetra-*N*-butyl ammonium hexafluorophosphate). Solutions were deoxygenated by vigorously degassing with N_2 for a minimum of 3 min with an N_2 flow presaturated with CH_3CN.

Materials. Solvents and chemicals were used as received unless otherwise noted. Solvents were obtained from Fisher Scientific; $TBAPF_6$ was from Oakwood Products Inc. The ligand 4-vinyl-4′-methyl-2,2′-bipyridine (vbpy) and the salt $[Fe(vbpy)_3](PF_6)_2$ and $[Zn(vbpy)_3](PF_6)_2$ were prepared as described in the literature.[8,17,18]

Instrumentation. Electrochemical experiments were conducted on a CH Instruments 660D potentiostat. All potential values are referenced to $Ag/AgNO_3$ (−0.12 V vs $FeCp^+/FeCp^0$) in CH_3CN 0.1 M in $TBAPF_6$ and to Ag/AgCl (+0.197 V vs NHE) in 0.5 M KNO_3. The $Ag/AgNO_3$ reference electrode solutions consisted of 0.1 M $TBAPF_6$ with 0.01 M $AgNO_3$ in CH_3CN while the Ag/AgCl consisted of ∼3 M NaCl in H_2O.

X-ray photoelectron spectra (XPS) were obtained at the Chapel Hill Analytical and Nanofabrication Lab (CHANL) at UNC. A Kratos Analytical Axis UltraDLD spectrometer with monochromatized X-ray Al Kα radiation (1486.6 eV) with an analysis area of 1 mm^2 was used. A survey scan was first performed with a step size of 1 eV, a pass energy of 80 eV, and a dwell time of 200 ms. High resolution scans were then taken for each element present with a step size of 0.1 eV and a pass energy of 20 eV. The binding energy for all peaks was referenced to the C 1s peak at 284.6 eV. To determine different oxidation states of the metals and different forms of C present on the surface, a Gaussian−Lorentzian curve fit with a Shirley (or occasionally linear) background subtraction was used. Quantitative data was obtained with application of empirical relative sensitivity factors. Sputter cleanings were accomplished by using an Ar^+ ion gun at 4 keV.

Surface morphology was characterized by atomic force microscopy (AFM) and scanning electron microscopy (SEM) with an energy dispersive X-ray spectrometer (EDS). For SEM measurements, samples were sputter coated with 3.0 nm of Au/Pd and imaged with an FEI Quanta 200 Field Emission Gun. EDS data were obtained on a FEI Helios 600 Nanolab Dual Beam System focused ion beam (FIB) equipped with an Oxford Instruments, INCA PentaFET−x3 X-ray detector with the electron beam set to 20 keV and a beam current of 0.69 nA. In addition, the ion beam was used to mill into the film and determine its permeability to the deposited metal particles. EDS measurements were made of film surfaces, and with a 1 μm^2, 100 nm

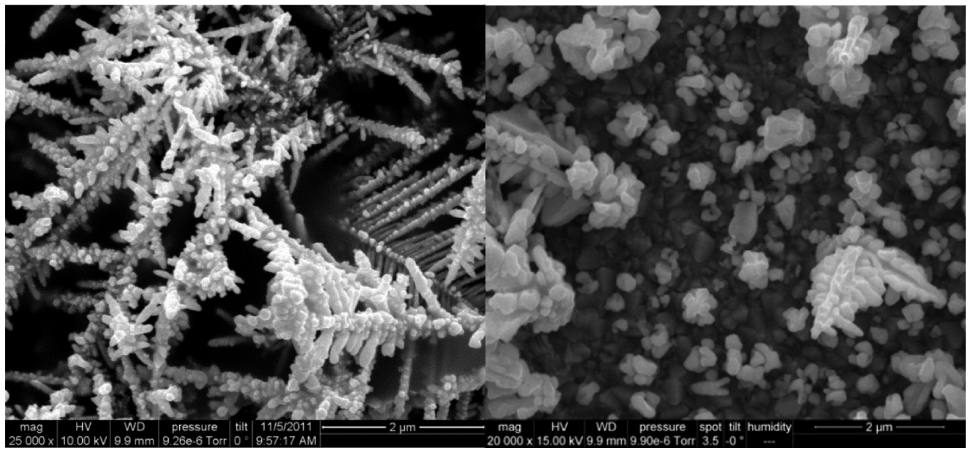

Figure 2. SEM of electrodeposited Ag on FTO by reductive cycling from 0 to −2 V vs $Ag/AgNO_3$ at 50 mV/s for 10 cycles (left) and following a potential hold at +0.04 V until ∼0.6 C had passed (less than 10 min) (right), with 10 mM $Ag(NO_3)$ and 0.1 M $TBAPF_6$ in CH_3CN. Note the smaller particles by reductive cycling.

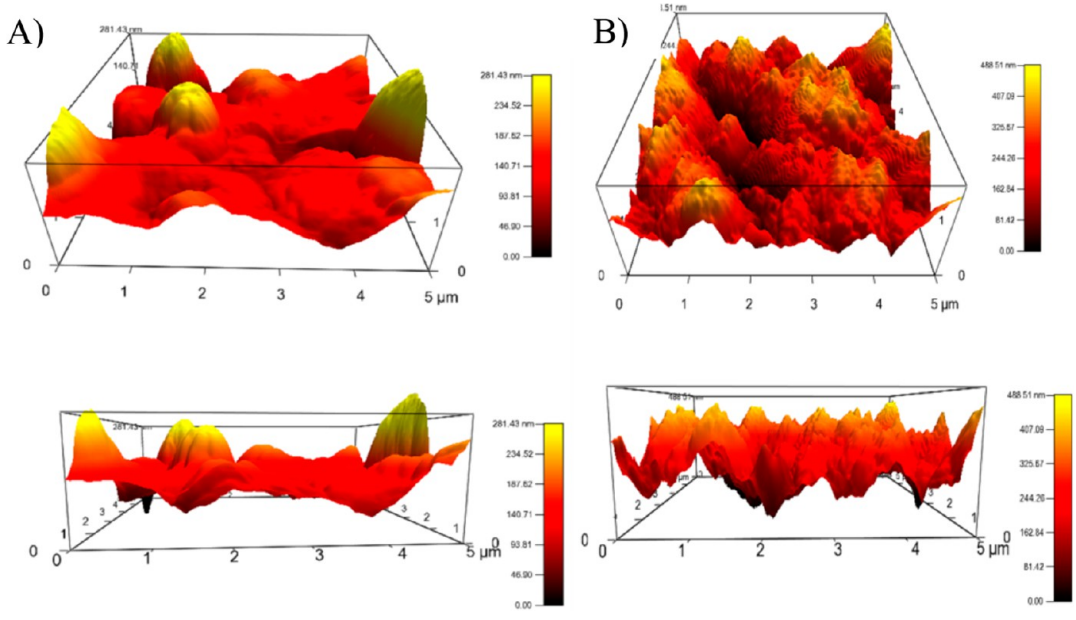

Figure 3. AFM data on (A) poly-$[Fe(vbpy)_3](PF_6)_2$ polymerized on FTO (left) compared to (B) after electrodeposition of Pt (right). Note the increase in surface roughness and evidence for film-embedded Pt particles.

deep square milled into the film, another EDS spectrum was recorded. AFM was used to qualitatively determine changes in surface roughness and topology after metal deposition. Images were obtained on an Asylum Research MFP3D AFM in AC mode. Scans were 5 μm^2 with a scan rate of 1.00 Hz.

Gas chromatography (GC) was performed on a SRI 8610C with a Multi-Gas #3 configuration and a 6 ft × 1/8 in. S.S. molecular sieve 13X packed column. A temperature gradient was used starting at 40 °C ramped to 220 °C at 15 °C/min. Gas samples were collected from the headspace of H^+ reduction reactions using a needle and syringe.

Preparation of Modified Electrodes. *(a). Preparation of Films of Poly-[Fe(vbpy)$_3$](PF$_6$)$_2$.* FTO electrodes were coated with films of poly-$[Fe(vbpy)_3](PF_6)_2$ by literature procedures.[17,18] The resulting pink films were rinsed with CH_3CN and allowed to dry in air. Surface coverages, Γ in mol/cm^2, of the electropolymers were estimated by using eq 1 where n is the number of electrons passed per redox couple (moles e^-), F is Faradays constant (96 485 C/mol), A is the area of the electrode (cm^2), and Q is the accumulated charge found by integrating the area under the $Fe^{III/II}$ anodic and cathodic peak couples.

$$\Gamma = \frac{Q}{nFA} \quad (1)$$

When 0.5 mM $[Fe(vbpy)_3](PF_6)_2$ in 0.1 M $TBAPF_6$/MeCN is cycled at 50 mV/s from −0.9 to −1.95 V vs $Ag/AgNO_3$, Γ ranges from 2.11 × 10^{-9} to 1.48 × 10^{-8} mol/cm^2 on approximately a 1.0 cm^2 FTO electrode. This correlated to film thicknesses of approximately 100−400 nm measured by SEM cross sectional imaging.

(b). Electrodeposition of Metals. Electrodepositions of M^0 particles was performed by reductive cycling from 0 to −2 V vs $Ag/AgNO_3$ at 50 mV/s for 2 cycles in 10 mM solutions of $Co(NO_3)_2$, $Ni(acac)_2$, $Cu(OAc)_2$, $PdCl_2(PhCN)_2$, $AgNO_3$, or $PtCl_2(PhCN)_2$ with 0.1 M $TBAPF_6$ in CH_3CN. Different scan windows, rates, and number of cycles were also examined but showed no significant advantages over those presented here. Each modified film was rinsed with CH_3CN and dried under standard atmospheric conditions prior to further analysis. The particles produced by reduction adsorb to bare FTO electrodes, even after thorough rinsing, as evidenced by SEM, EDS, and XPS. SEM shows a variety of surface morphologies, which are dependent on the metal used (Figure S1 of Supporting Information). Under these conditions, Ag and Pd deposit as small discrete particles ranging from

50 to 100 nm to 1−2 μm depending on the number of cycles, scan rate, and scan windows. More cycles, slower scan rates, and larger, more reductive scan windows resulted in longer deposition time and more extensive particle growth. Additionally, electrodepositions by holding electrodes at a fixed potential resulted in larger particles (Figure 2). Co, Ni, Cu, and Pt deposit as smaller submicrometer particles which together form thin metallic films.

Electrocatalysis. *(a). Electrocatalytic Reduction of H^+.* Electrodes were cycled reductively from +0.197 to −0.603 V vs NHE in 0.1 M $HClO_4$ with a Ag/AgCl reference electrode (+0.197 V vs NHE) and a Pt mesh counter. A clean FTO electrode was used to establish a baseline for H^+ reduction. Solutions were degassed with N_2 for 5 min before evaluation.

(b). Electrocatalytic Oxidation of H_2O. These experiments were carried out in 0.5 M KNO_3 (aq) buffered at pH 7 with added NaH_2PO_4 with a Ag/AgCl reference electrode and a Pt mesh counter electrode. A clean FTO electrode was used to establish a baseline.

RESULTS AND DISCUSSION

Electrodeposition. As noted below, Ag particles demonstrated a facility toward electrocatalytic H_2O oxidation, and different methods of applying reductive potentials for electrodeposition were investigated, including cycling the potential and controlled potential deposition at a fixed, negative value. SEM analysis showed that lower deposition potentials and longer deposition times led to smaller more evenly dispersed particles which, over longer electrodeposition times, grew into larger structures. Figure S1 (see Supporting Information) shows SEM images, and Figure 3 displays changes in surface morphology after polymerization and after metal deposition. Figure 2 illustrates the difference in particle size for reductive cycling compared to controlled potential deposition.

XPS was used to evaluate the oxidation state of the deposited metals. For Pt, Cu, Co, and Ni at least partial surface oxidation occurred after electrodeposition as shown by peak shapes and binding energies in XPS spectra for the Pt 4f and Cu, Co, and Ni 2p peaks. However, after a 30 s Ar^+ sputter cleaning treatment, nearly all surface metal oxides were removed with exposure of M^0. Example data from this procedure is shown in Figure S2 (see Supporting Information). On the basis of the time-resolved sputtering results, there is a buildup of MO_x on the surface of these structures with M^0 remaining beneath the surface, consistent with surface oxidation by oxygen. Ag and Pd are less prone to surface oxidation and remain as M^0.

Electrocatalytic H^+ Reduction to Hydrogen. As expected, Pt and Pd were the most efficient catalysts for reduction of H^+ to hydrogen. Current densities reached 18.3 and 13.2 mA/cm^2, respectively, when deposited on FTO, at −0.6 V vs NHE in 0.1 M $HClO_4$ in cyclic voltammetric (CV) scans with no observed plateau current. Current densities of 13.1 and 4.63 mA/cm^2 for Pt and Pd, respectively, were obtained upon deposition on poly-$[Fe(vbpy)_3](PF_6)_2$. Comparative electrolysis at −0.4 V vs NHE in 0.1 M $HClO_4$ with the two metals on FTO or in poly-$[Fe(vbpy)_3](PF_6)_2$ did not improve long-term stability for Pd but did slightly improve stability for Pt. Current loss was more rapid in the film but with higher current densities than for Pt on FTO at this potential (Figure 4). With Pd on FTO, the current density rose to 7 mA/cm^2 after ∼4 h at which point it dropped to ∼1.5 mA/cm^2 and remained constant indefinitely with obvious hydrogen evolution. Replacing the solution resulted in a return to current densities >7 mA/cm^2, Figure S3 (see Supporting Information). Pd deposited on poly-$[Fe(vbpy)_3](PF_6)_2$ showed little long-term catalytic activity. For Cu, Co, Ag, and Ni,

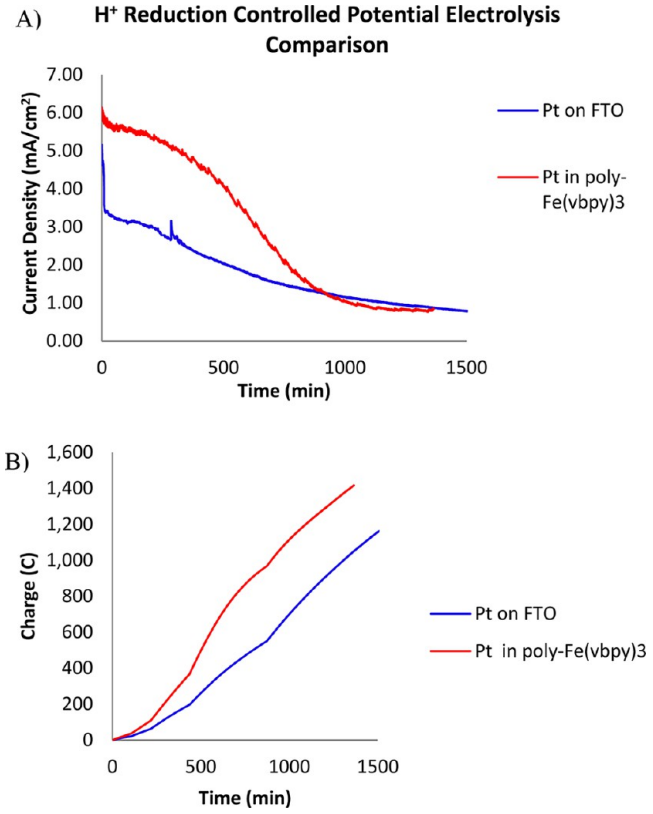

Figure 4. (A) Current density−time traces for hydrogen evolution at −0.4 V vs NHE in 0.1 M $HClO_4$; Pt on FTO compared to Pt in the polymer support. (B) Accumulated charge vs time trace for the same material as in (A).

maximum current densities on CV scans from +0.2 to −0.6 V reached 2.3, 0.96, 0.94, and 0.18 mA/cm^2 compared to a background current of 0.30 mA/cm^2, none of which showed a sign of a plateau current. Figures S4 and S5 (see Supporting Information) show CVs of the electrodes with the 6 different electrodeposited metals. GC analysis of the headspace verified H_2(g) formation.

Electrocatalytic H_2O Oxidation. Electrocatalytic H_2O oxidation was examined in aqueous solutions containing 0.5 M KNO_3 buffered at pH 7 with 0.1 M NaH_2PO_4/Na_2HPO_4. CVs of each metal-modified surface are shown in Figure S6 (see Supporting Information). Of significant note are the current enhancements for the Co and Ag modified electrodes. In oxidative scans, current densities reached 10.5 and 8.70 mA/cm^2, respectively, at +1.8 V vs NHE with onset potentials for the catalytic currents at ∼1.3 and ∼1.4 V, respectively. Visible gas evolution occurred just past the onset potentials and continued until, on negative scans, the potential was several hundred mV below the onset potential. For Pt, Pd, Cu, and Ni, current densities reached 6.0, 5.0, 2.0, and 1.4 mA/cm^2 respectively, all significantly enhanced compared to the background on FTO which reached 0.20 mA/cm^2 at +1.8 V vs NHE.

Initial enhancements in current density were observed on the poly-$[Fe(vbpy)_3](PF_6)_2$ support for electrodeposited Co, but oxidative currents decreased more rapidly than Co on FTO. For Ag particles, significant improvements in long-term electrocatalytic stability were observed. With the polymer support, the integrated charge passed over a 1000 min

electrolysis period, increased by ~25% compared to electrodeposited Ag on bare FTO (Figure 5 and 6).

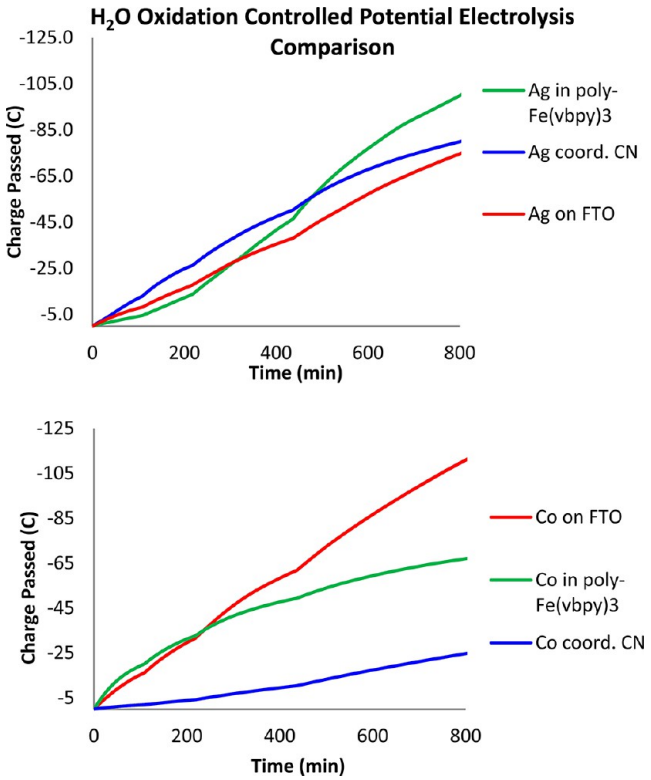

Figure 5. Long-term stability comparison of Co and Ag catalysts on FTO, in poly-$[Fe(vbpy)_3](PF_6)_2$, and coordinated to CN^- or free vbpy in poly-$Fe(vbpy)_2(CN)_2$,poly-vbpy in aqueous solution with 0.5 M KNO_3 buffered to pH 7 with 0.1 M NaH_2PO_4/Na_2HPO_4 at +1.6 V vs NHE.

Of particular interest were the electrocatalytic properties of Ag toward H_2O oxidation. After Ag electrodeposition, the electrode was cycled from −0.4 to 1.4 V vs $Ag/AgNO_3$ in CH_3CN in 0.1 M $TBAPF_6$. A CV of the resulting surface showed an increase in oxidative current at 0.18 V and a current plateau at 0.6 V. On the return scan, a reductive wave appeared at $E_{p,c}$ = −0.1 V (Figure S7 of Supporting Information).

Oxidative cycling in H_2O gave a similar $i-V$ response with an initial oxidative feature appearing on the first scan at $E_{p,c}$ = +0.64 V (Figure 7). With additional scans, the peak current at +0.64 V decreased accompanied by a shift in $E_{p,c}$ by 0.05 V. The reduction wave at $E_{p,c}$ = +0.01 V shifted positively by 0.03 V and decreased in current on further cycling. An increase in oxidative current occurs at +1.4 V accompanied by noticeable formation of oxygen on the surface. On the return scan, a new wave appears at $E_{p,a}$ = +1.2 V which also decreases in current upon further cycling.

Controlled potential electrolysis was carried out at +1.6 V vs NHE in a N_2(g) atmosphere glovebox with a fluorescense probe in the headspace to detect O_2. After 2 min O_2 levels rose above baseline, and after 2 h, the electrode was still evolving oxygen at a current density of 1.31 mA/cm^2 compared to 2.6 mA/cm^2 initially. An oxygen evolution−time trace is shown in Figure S8 (see Supporting Information).

The results for the electrodeposited metals on bare FTO are comparable to the results of other studies that utilized electrodeposited metal films as catalysts for H_2O oxidation.

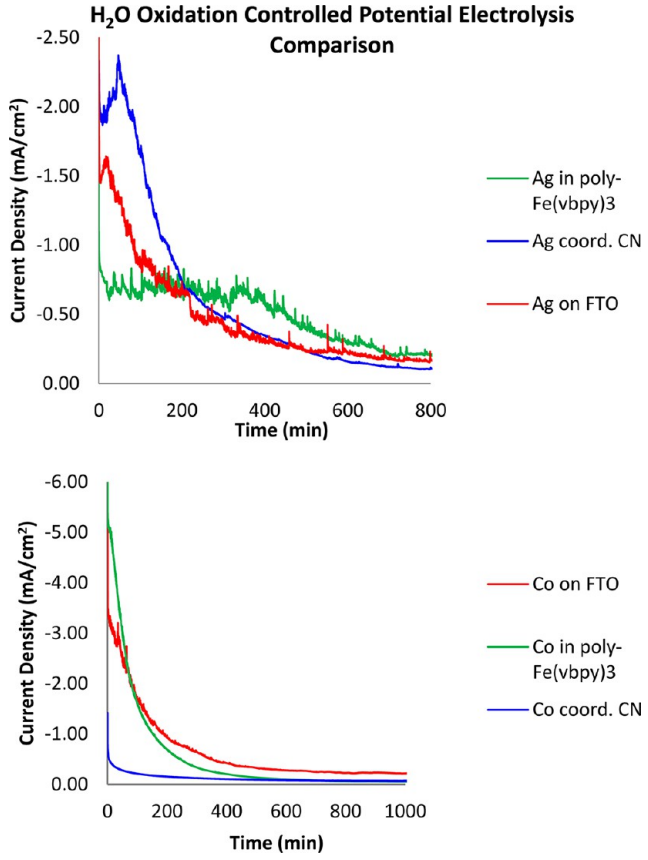

Figure 6. Long-term stability comparison of Co and Ag catalysts on FTO, in poly-$[Fe(vbpy)_3](PF_6)_2$, and Co(II) or Ag(I) coordinated to CN^- or free vbpy in poly-$Fe(vbpy)_2(CN)_2$,poly-vbpy in aqueous solution with 0.5 M KNO_3 buffered to pH 7 with 0.1 M NaH_2PO_4/Na_2HPO_4 at +1.6 V vs NHE.

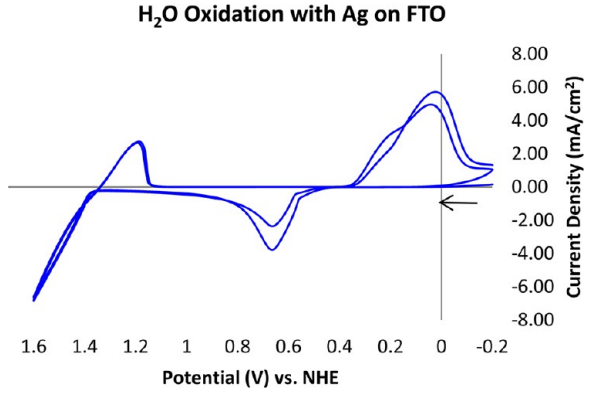

Figure 7. CV of Ag deposited on FTO (1 cm^2) in H_2O, pH 7 phosphate buffer with 0.5 M KNO_3 scanned in the positive direction.

Recent works have shown a variety of different electrodeposited metal oxides that are excellent catalysts for H_2O oxidation including Co, Ni, Mn, and Ir oxides.[21−25] In contrast to these works, the methods outlined here use reductive electrodepositions to generate a precursor metallic film or particles, that upon oxidative cycling (or an applied oxidative potential) will oxidize to the catalytically active species. The application of reductive electrodepositions by cycling the potential seems to generate more crack-resistant films, in an easy and straightforward manner. Other studies have found it difficult to identify proper deposition conditions;[23] however, using the method

dx.doi.org/10.1021/am401331k | ACS Appl. Mater. Interfaces 2013, 5, 7050−7057

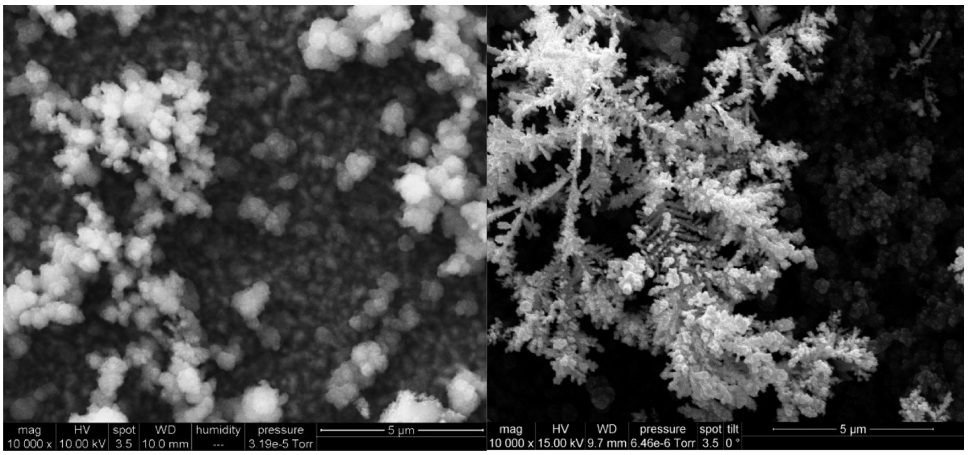

Figure 8. SEM of poly-$[Fe(vbpy)_3](PF_6)_2$ (left) with films approximately hundreds of nanometers thick which form large "popcorn" like mounds. Ag deposition on poly-$[Fe(vbpy)_3](PF_6)_2$ (right) resulted in Ag deposited both on the surface of the film (forming branch-like structures) and growing out from film.

outlined here, catalytically active films may be prepared under a variety of reducing conditions with comparable reactivity. One difference between the oxidative and reductive electrodeposition techniques is the overpotential required to oxidize H_2O. Although several studies have been conducted at acidic[25] and basic[24] pH, making direct comparison difficult, comparisons may be drawn at neutral pH. For the Co oxide catalyst reported by Nocera and co-workers,[21] onsets are reported at 1.23 V compared to 1.3 V for the reductively deposited Co catalyst reported here. In addition, for the oxidatively deposited Mn oxide catalyst reported by Dau and co-workers,[23] an onset of 1.2 V is reported under similar conditions. Although there are some benefits to oxidatively deposited catalysts, such as the ability to form in situ, the resultant films are oftentimes cracked and inconsistent, as well as difficult to deposit in the case of some metals such as Mn.[23]

Reactivity of Metal Particles in Electropolymerized Films Toward H_2O Oxidation. Enhanced stability in the electropolymerized films toward H_2O oxidation was also investigated. These experiments utilized electropolymerized films of $[Fe(vbpy)_3](PF_6)_2$ and $[Zn(vbpy)_3](PF_6)_2$ on FTO electrodes with preparation and properties described above.[6−19] Following electropolymerization, the films were cycled reductively in solutions containing the metal ions under the same conditions as on bare FTO as described above. Because the polymers are electrically conductive in potential regions defined by metal- and ligand-based redox couples and are semiporous, metal ions can diffuse into the interior where, at negative potentials, they are reduced within the film, on the surface, and at the electrode−film interface. Films of poly-$[Fe(vbpy)_3](PF_6)_2$ can be readily converted to poly-Fe-$(vbpy)_2(CN)_2$,poly-vbpy with metal-ion binding sites at the uncoordinated vbpy and Fe-CN.[6,7] The Zn(II) ion, in films of poly-$[Zn(vbpy)_3](PF_6)_2$, is substitutionally labile and can be exchanged with metal ions such as Co^{2+}, which are themselves redox active and act as sites for electrocatalysis.[8]

Several experiments were conducted to verify that the metal ions were successfully reduced and incorporated into the polymer film network. SEM shows clear deposition of metal particles on the surface of the polymer; these particles appear to not only be adsorbed to the polymer but also embedded within this semiporous network. Particularly intricate structures were produced with electrodeposited Ag creating high surface area branched structures during reductive cycles, Figure 8.

FIB methods were used to mill 1 μm^2 square portions of film samples approximately 0.1 μm deep. With a sample of poly-$[Fe(vbpy)_3](PF_6)_2$ that had been reductively cycled in a Pt^{2+} solution, an EDS attachment was used to collect spectra before and after milling. The amount of Fe detected decreased from 0.66% before milling to 0.34% after milling, while the amount of Pt decreased from 1.45% to 0.63% but was maintained throughout the milling process. These data show that, while the majority of the material deposits on the surface, the semiporous films allow for diffusion and reduction of Pt(II) within the film which agrees with prior studies.[19]

AFM data were also collected on poly-$[Fe(vbpy)_3](PF_6)_2$ before and after Pt electrodeposition. The results of these experiments showed a significant increase in surface roughness after electrodeposition, with particles ∼30−80 nm in size embedded in the film, Figure 3.

Improvements to Long-Term Stability. For both H^+ reduction and H_2O oxidation, poly-$[Fe(vbpy)_3](PF_6)_2$ with electrodeposited metals generally exhibits slightly larger overpotentials and lower current densities compared to electrodeposited metals on FTO. However, in some instances, catalysis was sustained for longer periods in poly-$[Fe(vbpy)_3]$-$(PF_6)_2$ films relative to FTO. The stabilization effect is likely due to its semiporous nature and ability to support the deposition of metal particles in a structured matrix.

Stabilization of electrodeposited Ag for H_2O oxidation was especially notable. Relatively constant oxidative current densities were observed at ∼0.6−0.8 mA/cm^2 for the first 6 h of electrolysis compared to a rapid decrease in current when deposited on FTO. Additionally, Figures 5 and 6 compare charge and current passed during controlled potential H_2O oxidation electrolysis for Co and Ag electrodeposited on FTO, in poly-$[Fe(vbpy)_3](PF_6)$, and coordinated to CN^- or free vbpy in poly-$Fe(vbpy)_2(CN)_2$,poly-vbpy.

Electrocatalysis in Films of Poly-$[M(vbpy)_3](PF_6)_2$. During a CV scan of poly-$[Zn(vbpy)_3](PF_6)$ from 1.6 to −1.8 V vs $Ag/AgNO_3$ in CH_3CN, a bpy reduction wave is observed at −1.64 V. After soaking in 10 mM $Co(NO_3)_2$ in CH_3CN overnight, the CV included a new reduction wave at −1.14 V vs $Ag/AgNO_3$, attributable to reduction of Co(II). Soaking a second film in 10 mM $Cu(OAc)_2$ in CH_3CN

followed by cyclic voltammetry showed a Cu(II) reduction wave at −1.09 V vs $Ag/AgNO_3$. Similarly, soaking a third film in 10 mM $FeCl_2$ generates poly-$[Fe(vbpy)_3](PF_6)_2$. All four CVs are shown in Figure S9 (see Supporting Information). Similar observations were made previously except for Cu(II) incorporation.[20] SEM measurements revealed formation of a thin polymer film on the FTO electrode after the polymerization step suggesting that films of poly-$[Zn(vbpy)_3](PF_6)_2$ are transparent and much thinner than films of poly-$[Fe(vbpy)_3](PF_6)_2$ (Figure S10, Supporting Information).

Polymer films after Zn^{2+} exchange exhibited greatly enhanced electrocatalytic H_2O oxidation compared to the FTO background. During a CV from +0.2 to +1.8 V, current densities for the Cu(II) and Co(II) exchanged films reached 2.2 and 6.0 mA/cm^2, respectively (Figure S11, Supporting Information). However, catalytic currents during controlled potential electrolysis were not sustained for periods as long as those found for the electrodeposited metals either on FTO or in poly-$[Fe(vbpy)_3](PF_6)$.

We have applied a number of metrics to compare catalytic efficiencies and stabilities for the various substrate−particle combinations with a summary given in Table 1. For H_2O oxidation, peak current densities at +1.8 V, as obtained from CVs, are listed. The time required to reach 10% of this initial current density at +1.6 V vs NHE at pH 7 with 0.5 M KNO_3 was chosen as the end of effective H_2O oxidation catalysis. These results, with total Coulombs passed after 1000 min, showed that Co on FTO is the most active metal toward H_2O oxidation with a notable decrease for Co in poly-$[Fe(vbpy)_3](PF_6)_2$. However, Ag deposited on poly-$[Fe(vbpy)_3](PF_6)_2$ maintained a constant current for ∼6 h with a ∼25% increase in charge passed after 1000 min. Similar metrics are summarized for proton reduction in Table 2.

Table 1. Summary of Electrocatalytic H_2O Oxidation Current Densities and Stabilities[a]

sample	current density (mA/cm^2) at +1.8 V	time to reach 10% of the initial peak current at +1.6 V (min)	charge passed after 1000 min (C)
Co on FTO	13.0	156	130
Co in poly-$Fe(vbpy)_3^{2+}$	13.2	110	75.7
Co(II) coordinated to CN[b]	3.12	35.8	35.7
Ag on FTO	11.7	79.0	94
Ag in poly-$Fe(vbpy)_3^{2+}$	3.90	515	123
Ag(I) coordinated to CN[b]	4.47	360	95.1
Co(II) exchanged in poly-$Zn(vbpy)_3^{2+}$	6.0	1.2	23.7
poly-$Zn(vbpy)_3^{2+}$	0.08	0	2.1
FTO	0.11	0	3.1

[a]Current densities were determined by CV measurements. Time to reach 10% of initial peak current at +1.8 V vs NHE and integrated charge passed after 1000 min was obtained by controlled potential electrolysis at +1.6 V. [b]Coordinated to −CN or free vbpy in poly-$Fe(vbpy)_2(CN)_2$,poly-vbpy.

Table 2. Comparison of the Long-Term Stability of Pt for Electrocatalytic Proton Reduction Deposited on Various Substrates

sample	current density (mA/cm^2) at −0.6 V	time to reach 10% of the initial peak current at −0.4 V (min)	charge passed after 1000 min (C)
Pt on FTO	8.59	1387	699
Pt in poly-$Fe(vbpy)_3^{2+}$	10.3	1014	1110
FTO	0.31	0.43	0.18

CONCLUSIONS

We have demonstrated that electroactive metal particles can be embedded inside electropolymerized films of poly-$[Fe(vbpy)_3](PF_6)_2$ and analyzed by use of electrochemical and surface analysis measurements. The resulting hybrid structures exhibit activity toward H_2O oxidation and H^+ reduction, albeit at significant overpotentials. Reductive electrodeposition on unmodified FTO surfaces resulted in catalytically active surface structures with relatively high stabilities. Pt and Pd on FTO showed impressive current densities toward H^+ reduction to hydrogen while Co and Ag were catalytically active toward H_2O oxidation. These directly electrodeposited films are of comparable reactivity to other electrodeposited catalysts for H_2O oxidation with the added benefit of producing more consistent, crack-resistant films.[21−25] In addition, improvements in long-term stability are seen in some instances with the poly-$[Fe(vbpy)_3](PF_6)_2$ support. With electropolymerized films of poly-$[Zn(vbpy)_3](PF_6)_2$, simple metal ion displacement provides a basis for preparing redox active films of poly-$[M(vbpy)_3](PF_6)_2$, where M = Co^{2+} or Cu^{2+} which also demonstrated reactivity toward electrocatalytic H_2O oxidation. Stabilization of Ag as a H_2O oxidation electrocatalyst in the film environment is a notable result, perhaps opening a door to a general procedure for stabilizing electrocatalytically active metal particles and clusters and utilizing these hybrid structures in catalytic applications. We are currently extending this work to electrocatalytic CO_2 reduction.

ASSOCIATED CONTENT

Supporting Information

SEM, CVs, controlled potential electrolysis graphs, and XPS spectra. This information is available free of charge via the Internet at http://pubs.acs.org/.

AUTHOR INFORMATION

Corresponding Author

*E-mail: tjmeyer@unc.edu.

Notes

The authors declare no competing financial interest.

ACKNOWLEDGMENTS

The authors acknowledge support from the U.S. Department of Energy, Office of Science, Office of Basic Energy Sciences, under Award Number DE-FG02-06ER15788. Also, we express our thanks to CHANL staff, Dr. Amar Kumbhar, and Dr. Carrie Donley for their assistance in collecting SEM, FIB, EDS, AFM, and XPS data.

ABBREVIATIONS

FTO, fluorine-doped tin oxide
vbpy, 4-methyl-4′-vinyl-2,2′-bipyridine

$TBAPF_6$, tetra-*N*-butyl ammonium hexafluorophosphate
SEM, scanning electron microscopy
AFM, atomic force microscopy
XPS, X-ray photoelectron spectroscopy
CV, cyclic voltammogram
FIB, focused ion beam
GC, gas chromatography
NHE, normal hydrogen electrode

REFERENCES

(1) Cook, T. R.; Dogutan, D. K.; Reece, S. Y.; Surendranath, Y.; Teets, T. S.; Nocera, D. G. *Chem. Rev.* **2010**, *110*, 6474.
(2) Meyer, T. J. *Nat. Chem.* **2011**, *3*, 757.
(3) Nocera, D. G. *Inorg. Chem.* **2009**, *48*, 10001.
(4) Nocera, D. G. *Acc. Chem. Res.* **2012**, *45*, 767.
(5) Barber, J. *Chem. Soc. Rev.* **2009**, *38*, 185.
(6) Calvert, J. M.; Schmehl, R. H.; Sullivan, B. P.; Facci, J. S.; Meyer, T. J.; Murray, R. W. *Inorg. Chem.* **1983**, *22* (15), 2151−2162.
(7) Leidner, C. R.; Sullivan, B. P.; Reed, R. A.; White, B. A.; Crimmins, M. T.; Murray, R. W.; Meyer, T. J. *Inorg. Chem.* **1987**, *26* (6), 882−891.
(8) Moss, J. A.; Argazzi, R.; Bignozzi, C. A.; Meyer, T. J. *Inorg. Chem.* **1997**, *36* (5), 762−763.
(9) O'Toole, T. R.; Margerum, L. D.; Westmoreland, T. D.; Vining, W. J.; Murray, R. W.; Meyer, T. J. *J. Chem. Soc., Chem. Commun.* **1985**, No. 20, 1416−1417.
(10) Ramos Sende, J. A.; Arana, C. R.; Hernandez, L.; Potts, K. T.; Keshevarz-K, M.; Abruna, H. D. *Inorg. Chem.* **1995**, *34* (12), 3339−3348.
(11) Cosnier, S.; Deronzier, A.; Moutet, J.-C. *J. Mol. Catal.* **1988**, *45* (3), 381−391.
(12) Abruna, H. D.; Denisevich, P.; Umana, M.; Meyer, T. J.; Murray, R. W. *J. Am. Chem. Soc.* **1981**, *103* (1), 1−5.
(13) Bakir, M.; Mackay, S. G.; Linton, R. W.; Sullivan, B. P.; Meyer, T. J. *Inorg. Chem.* **1994**, *33* (18), 3945−3951.
(14) Bakir, M.; Sullivan, B. P.; MacKay, S. G.; Linton, R. W.; Meyer, T. J. *Chem. Mater.* **1996**, *8* (10), 2461−2467.
(15) Meyer, T. J.; Sullivan, B. P.; Caspar, J. V. *Inorg. Chem.* **1987**, *26*, 4145.
(16) Murray, R. W. *Annu. Rev. Mater. Sci.* **1984**, *14*, 145−169.
(17) Abruna, H. D.; Denisevich, P.; Umafia, M.; Meyer, T. J.; Murray, R. W. *J. Am. Chem. Soc.* **1981**, *103*, 1.
(18) Denisevich, P.; Abruna, H. D.; Leidner, R. C.; Meyer, T. J.; Murray, R. W. *Inorg. Chem.* **1982**, *21*, 2153.
(19) MacKay, S. G.; Bakir, M.; Mussleman, I. H.; Meyer, T. J.; Linton, R. W. *Anal. Chem.* **1991**, *63*, 60.
(20) Mohanty, U. S. *J. Appl. Electrochem.* **2011**, *41*, 257−270.
(21) Kanan, M. W.; Nocera, D. G. *Science* **2008**, *321*, 1072−1075.
(22) Dinca, M.; Surendranath, Y.; Nocera, D. G. *Proc. Natl. Acad. Sci. U.S.A.* **2010**, *107*, 10337−10341.
(23) Zaharieva, I.; Chernev, P.; Risch, M.; Klingan, K.; Kohlhoff, M.; Fischer, A.; Dau, H. *Energy Environ. Sci.* **2012**, *5*, 7081−7089.
(24) Gorlin, Y.; Jaramillo, T. F. *J. Am. Chem. Soc.* **2010**, *132*, 13612−13614.
(25) Blakemore, J. D.; Schley, N. D.; Kushner-Lenhoff, M. N.; Winter, A. M.; D'Souza, F.; Crabtree, R. H.; Brudvig, G. W. *Inorg. Chem.* **2012**, *51*, 7749−7763.
(26) Cobo, S.; Heidkamp, J.; Jacques, P. A.; Fize, J.; Fourmond, V.; Guetaz, L.; Jousselme, B.; Ivanova, V.; Dau, H.; Palacin, S.; Fontecave, M.; Artero, V. *Nat. Mater.* **2012**, *11*, 802.
(27) Ochmanska, J.; Pickup, P. G. *J. Electroanal. Chem.* **1989**, *271*, 83−105.